J Appl Electrochem (2009) 39:1925–1938
DOI 10.1007/s10800-009-9901-7

ORIGINAL PAPER

Novel catalyst-support interaction for direct formic acid fuel cell anodes: Pd electrodeposition on surface-modified graphite felt

Tommy T. Cheng · Előd L. Gyenge

Received: 27 November 2008 / Accepted: 14 April 2009 / Published online: 29 April 2009

Abstract The electrodeposition of Pd on graphite felt (GF, thickness ~3 mm in uncompressed state) was studied and the resulting catalyst was compared with Pt-Ru/GF for the electro-oxidation of formic acid. A micellar solution composed of the non-ionic surfactant Triton X-102 and an aqueous phase containing $PdCl_2$ were utilized for the galvanostatic electrodeposition of Pd nanoparticles. The presence of the surfactant during electrodeposition coupled with pretreatment of the GF surface by a Shipley-type method ($PdCl_2 + SnCl_2$ solution) creating nucleation sites had a major impact on the Pd catalyst morphology and penetration throughout the electrode thickness, affecting, therefore, the electrocatalytic activity toward formic acid oxidation. It was found that large (~1,000 nm) Pd particles with smooth surface favored the indirect CO_{ad} pathway, while Pd nanoparticles (diameter <40 nm) with rough surface, formed with surfactant and pretreatment, were much more active leading to the direct non-CO_{ad} pathway. Due to pretreatment the GF surface has been modified and the effective catalytic system could be described as Pd/SnO_2–Pd(PdO)/GF with possible electronic interaction between support and catalyst. In direct formic acid fuel cell (DFAFC) experiments at 333 K and 1 M HCOOH, the peak power density using the Pd/GF anode reached 852 W m^{-2} (57 g m^{-2} Pd) compared to 392 W m^{-2} (40 g m^{-2} Pd) with a commercial Pd catalyst-coated membrane (CCM). The long-term stability of Pd-based anodes was poor and inferior to Pt–Ru (4:1 at. ratio) prepared and tested under identical conditions.

T. T. Cheng · E. L. Gyenge (✉)
Department of Chemical and Biological Engineering,
The University of British Columbia, 2360 East Mall,
Vancouver, BC V6T 1Z3, Canada
e-mail: egyenge@chml.ubc.ca

Keywords Electrocatalyst · Direct formic acid fuel cell · Electrodeposition · Porous electrode · Extended reaction zone anode

1 Introduction

The direct formic acid fuel cell (DFAFC) has been shown to be an excellent candidate for powering portable electronic devices. The DFAFC has not only a higher thermodynamic cell voltage (1.45 V) than the direct methanol fuel cell (DMFC, 1.19 V), but also possesses a smaller crossover flux due to electrostatic repulsion between $HCOO^-$ and the $-SO_3^-$ groups in the Nafion® membrane, resulting in higher fuel utilization and less severe cathode contamination [1–3].

It is generally accepted that the electro-oxidation of formic acid on Pt proceeds through a dual-path mechanism originally proposed by Capon and Parsons in 1973, involving a non-CO direct path and a CO indirect pathway [4–7]. The direct path proceeds via dehydrogenation and CO_2 is formed through active non-CO_{ad} intermediates. The indirect path involves the formation of adsorbed carbon monoxide, both an intermediate and a catalyst poison, through dehydration. The adsorbed carbon monoxide can be subsequently oxidized on Pt to CO_2 at potentials higher than about 0.5 V_{RHE}.

The electro-oxidation of formic acid on Pd is believed to proceed primarily through a non-CO pathway [8]. Partial evidence was obtained by CO stripping voltammetry, revealing that the CO accumulation on Pd black was significantly lower than on Pt black [9]. Furthermore, it was shown by Arenz et al. [10] that no adsorbed CO could be detected on Pd by Fourier Transform Infrared

Spectroscopy (FTIR) even though a high production rate of CO_2 was observed. As a result, Pd has better performance than Pt, especially at low anode potentials (<0.4 V_{RHE}) where the adsorbed CO intermediate on Pt cannot be further oxidized. However, it is important to note that Pd deactivates during formic acid oxidation [2, 9–11]. Blair et al. [11] have published chronopotentiometry data on the long-term stability of Pt, Pd, and various Pd–Pt catalysts. It was found that the Pd activity, although initially substantially higher compared to Pd–Pt alloys, falls below the activity of Pd–Pt and Pt within about 6 h. Li and Hsing [2] reported higher Pd deactivation rate, the formic acid oxidation current decreased by a factor of 10 over a 30 min period. The Pd deactivation during formic acid oxidation is not well understood at present and more studies are required to elucidate its mechanism. According to Arenz et al. [10], Pd deactivation could be due to poisoning of the formic acid oxidation active sites (e.g., specific crystal planes) by 'spectator' species such as H_{ad} and OH_{ad}, and anions from the supporting electrolyte (e.g., SO_4^{2-}). Furthermore, the Pd particle size, crystallographic features, and surface morphology might play a role as well. A typical Pd reactivation procedure involves anode potential spiking to 1.2 V_{RHE} for a few seconds [12].

The DFAFC anode structure has also received research attention particularly aimed at improving the utilization of the catalyst load. Wilkinson et al. [13] and Gyenge et al. [14–18] showed the benefits of extending the anode reaction zone in direct liquid fuel cells by employing either a multi-layer [13] or a one-piece porous electrode such as catalyzed reticulated vitreous carbon, various graphite felts, and titanium mesh [14–18]. Using 10 g m^{-2} Pt–Ru catalyst supported on un-pressed graphite felt (GF) as anode, the peak power density of a DMFC operated at 333 K reached 741 W m^{-2} compared to 442 W m^{-2} obtained with a commercial gas diffusion Pt–Ru anode with identical catalyst load but dispersed/supported on the carbon diffusion layer [18]. The same Pt–Ru/GF anode was also employed in a DFAFC, where the peak power density at 333 K was 860 W m^{-2} versus 528 W m^{-2} generated with a commercial Pt–Ru catalyst-coated membrane (CCM). Thus, the extended reaction zone electrode was more effective than the gas diffusion electrode in either the catalyst-coated diffusion layer or catalyst-coated membrane configurations. The performance enhancement has been attributed to a combination of factors: better catalyst utilization, improved fuel mass transfer, and more effective $CO_{2,(g)}$ disengagement from the anode. In addition, Chetty and Scott [19] have demonstrated the use of Ti mesh as DFAFC anode support for thermally deposited Pd and Pt–Sn catalysts.

The goal of the present investigation was twofold. First, to investigate the effect of graphite surface pretreatment in conjunction with our previously developed catalyst preparation method, namely electrodeposition from Triton X-102 micellar solution [18], for the synthesis and uniform dispersion of Pd nanoparticles throughout the three-dimensional GF electrode. Second, to study the electrocatalytic activity of the Pd/GF for HCOOH oxidation in comparison with Pt–Ru/GF by both half-cell and fuel cell experiments.

2 Experimental methods

2.1 Graphite felt pretreatment with Shipley-type method

The GF (thickness 3 mm in uncompressed state) was provided by Test Solutions through Electrolytica Inc. It was produced by graphitization of polyacrylonitrile based carbon fibers. The GF substrate had a surface area of 0.7 m^2 g^{-1} (measured by BET N_2 adsorption) and carbon content of 99.7 wt%. Due to the very high graphitic carbon content, the surface oxygen concentration associated with functional groups of the un-pretreated GF is low, about 4.8 at.% (Table 1, first entry). The 5 cm^2 geometric area GF substrates were first sonicated in methanol for 30 min followed by thorough washing in distilled water. Afterward, a graphite surface sensitization and pretreatment step was performed for selected samples. This step involved the immersion of GF in a $PdCl_2$ (6 mM) + $SnCl_2$ (0.3 M) solution for up to 48 h at 303 K. The $PdCl_2$ + $SnCl_2$ pretreatment solution (referred to also as a Shipley-type solution [16, 20]), was prepared by mixing 0.1 g of $PdCl_2$ (Sigma-Aldrich), 5 g of $SnCl_2 \cdot 2H_2O$ (Sigma-Aldrich), 60 mL of de-ionized water, and 30 mL of 37.5 wt% HCl (Fisher Scientific). After the pretreatment method was completed, the samples were washed thoroughly again with distilled water followed by drying in air.

The Shipley-type pretreatment is based on the surface redox reactions of carbon, Pd^{2+}, and Sn^{2+} ions (Eqs. 1–4). The Pd^{2+} ions are spontaneously reduced to Pd (Eq. 1) with the coupled oxidation of: (i) Sn^{2+} to SnO_2 (Eq. 2) or Sn^{4+} (Eq. 3) and (ii) the potential oxidation of carbon creating oxidized surface functional groups (–COH, –CO, –CHO, –COOH,) and CO_2 (Eq. 4).

Thus, the metallic species formed on the GF surface as a result of the Shipley treatment are Pd and SnO_2. The formation of elemental Sn (Eq. 5) is unlikely based on the redox chemistry. Some of the deposited Pd could be oxidized to PdO (Eq. 6) by the O_2 present in solution (Eq. 7). Surface analysis was performed to confirm the proposed redox chemistry (see Sect. 2.4).

Table 1 The effect of Shipley solution (6×10^{-3} M $PdCl_2$—0.3 M $SnCl_2$—4 M HCl) pretreatment on graphite felt (GF) at 303 K

Pretreatment time (h)	Pd (g m^{-2})	Sn (g m^{-2})	Deposition yield (wt%)	Pd surface content (at.%)	Sn surface content (at.%)	Oxygen surface content (at.%)
0	0	0	0	0	0	4.8
24	0.6	0.7	Pd: 2.0% Sn: 0.04%	2.4	8.2	26.6
48	1.0	0.8	Pd: 3.3% Sn: 0.05%	3.9	10.0	33.5

$$Pd^{2+} + 2e^- \leftrightarrow Pd \qquad E^0_{298} = 0.85\ V_{SHE} \qquad (1)$$

$$SnO_2 + 4H^+ + 2e^- \leftrightarrow Sn^{2+} + 2H_2O \quad E^0_{298} = -0.09\ V_{SHE} \qquad (2)$$

$$Sn^{4+} + 2e^- \leftrightarrow Sn^{2+} \quad E^0_{298} = 0.15\ V_{SHE} \qquad (3)$$

$$CO_2 + 4e^- + 4H^+ \leftrightarrow C_{[graphite]} + 2H_2O \quad E^0_{298} = 0.21\ V_{SHE} \qquad (4)$$

$$Sn^{2+} + 2e^- \leftrightarrow Sn \quad E^0_{298} = -0.14\ V_{SHE} \qquad (5)$$

$$PdO + 2H^+ + 2e^- \leftrightarrow Pd + H_2O \quad E^0_{298} = 0.70\ V_{SHE} \qquad (6)$$

$$O_2 + 4H^+ + 4e^- \leftrightarrow 2H_2O \quad E^0_{298} = 1.23\ V_{SHE} \qquad (7)$$

2.2 Pd electrodeposition procedure

The Pd electrodeposition solution was composed of up to 25 vol% Triton X-102 non-ionic surfactant [$C_8H_{17}C_6H_4O(C_2H_4O)_{12}H$], and the rest was an aqueous phase containing $PdCl_2$. The concentration of $PdCl_2$ in the micellar solution varied between 0.75 mM and 4.5 mM (i.e., millimolar). No additional electrolyte was used during electrodeposition. The critical micelle concentration of Triton X-102 is 0.33 mM and its HLB number (hydrophile-lypophile balance) is 14.6 [21]. Since HLB > 13, it indicates very good dispersibility in water and excellent surface wetting properties, both essential characteristics for electrodeposition. The chemicals were reagent grade obtained from Sigma-Aldrich and were used as delivered without further purification processes. The micellar solution was prepared by mixing the aqueous and surfactant phases for 30 min at 341 K in a water-jacketed glass vessel connected to a circulating water bath.

The electrode assembly consisted of the GF working electrode placed at about 1 cm between two perforated platinized titanium counter electrodes (anodes), each with a geometric surface area of 5 cm^2 (with ~10 holes per cm^2 and hole dimensions of ~0.3 cm^2). We described in a previous publication the benefits of using perforated counter electrodes during electrodeposition on 3-D substrates [17]. The electrodes were inserted into the water-jacketed glass vessel containing the $PdCl_2$ micellar solution and the electrodeposition was carried out in galvanostatic mode under well-mixed conditions. A Xantrex XHR150-7 DC power supply was employed capable of operating at 0–150 V and 0–7 A.

After the electrodeposition was completed, the GF was sonicated in tetrahydrofuran (THF) (Reagent Grade, Sigma Aldrich) for 5 min to wash out the surfactant retained in the GF electrode. Next the GF was thoroughly washed with distilled water and dried in air followed by heat treatment in an inert atmosphere (i.e., N_2 stream) for 1 h at 573 K to remove traces of adsorbed organic compounds. After the post-deposition thermochemical treatment and before the electrochemical experiments, the Pd/GF was also subjected to electrochemical conditioning by applying three potential steps of 1.28, 1.20, and 0.05 V versus SHE for 10 s each, repeated three times. The effects of post-deposition thermochemical and electrochemical treatments were discussed in a previous publication [16].

2.3 Half-cell electrochemical experiments

Electrochemical measurements, including cyclic voltammetry (CV) and chronoamperometry (CA) were carried out at 298 K in a water-jacketed electrochemical cell connected to a circulating water bath. The test assembly was composed of a three-electrode setup: Hg/Hg_2SO_4, K_2SO_4std. (MSE) reference electrode, platinum wire as counter electrode, and the GF of interest as working electrode. The electrolyte was either 1 M or 3 M HCOOH mixed with 0.5 M H_2SO_4. A Radiometer Analytical VoltaLab PGZ402 potentiostat with the VoltaMaster 4 software was used in all experiments. All potentials in the present work are reported against the standard hydrogen electrode (SHE) reference.

The electrochemically active Pd surface area was estimated using Cu underpotential (UPD) a technique that was shown to be effective for Pt–Ru deposited on reticulated vitreous carbon, GF, and Ti mesh [16–18]. Cu UPD has been also employed by Rusanova et al. [22] to determine the surface area of Pd electrodeposits. Therefore, in the present

study the effective surface area was estimated from the anodic stripping charge of a monolayer of Cu (i.e., 4.2 C m^{-2}). The Cu UPD experiments were carried out in 0.5 M H_2SO_4 and 2 mM $CuSO_4$ at 298 K. Prior to Cu UPD, reference voltammograms between the potential range of −0.04 to 0.91 V were obtained in 0.5 M H_2SO_4 at a scan rate of 50 mV s^{-1}. A monolayer of Cu was underpotential deposited on the catalyst surface by polarizing the GF at 0.26 V for 300 s. An anodic linear voltammetric scan at 50 mV s^{-1} was then applied from 0.26 to 0.91 V to remove the adsorbed Cu. The charge differences between the reference and anodic linear scan were used to calculate the active surface area.

2.4 Surface and analytical characterization of the Pd catalysts

A Hitachi S4700 high-resolution SEM instrument with an accelerating voltage and emission current of 2,000 V and 1.25×10^7 A, respectively, was employed. Fragments of the Pd/GF were flush mounted onto SEM stubs with carbon adhesive and a working distance of 2.5–3.5 mm was employed. A Hitachi S4500 field-emission scanning electron microscope (FESEM) using a 5,000 V electron beam voltage was also used to capture high-resolution images of selected samples.

The Pd mass load on GF was determined by ICP-AES using a Perkin Elmer Optima, model 3300DV instrument. Pd/GF samples with a geometric area of 1 cm^2 were weighed and digested in Aqua Regia for 4 h to dissolve completely the Pd deposit. The resulting solution was then diluted and the Pd content was determined by ICP-AES.

The crystallographic features of the Pd catalysts were determined by XRD using an Advanced Bruker powder X-ray diffractometer with Cu K radiation wavelength of 1.5418 Å. The XRD experiments were performed with 2θ values from 10° to 85° with a stepping of 0.04°.

The GF substrates pretreated with Shipley solution were analyzed by XPS using a Kratos Axis Ultra spectrometer with a probing depth of 7–10 nm, and detection limits ranging from 0.1 to 0.5 at.% depending on the element. Survey scan spectra were obtained from an analysis area of $\sim 0.300 \times 0.700$ nm in size and with a pass-energy of 160 eV. High-resolution spectra were obtained with a pass-energy of 10 eV.

2.5 Membrane electrode assembly and fuel cell experiments

Membrane electrode assemblies (MEA) with effective electrode area of 5 cm^2 were utilized in DFAFC experiments. In order to test the Pd/GF prepared in the present work half-MEA (i.e., without Pd black anode) was provided by Lynntech Inc. containing 40 g m^{-2} of Pt black (cathode) coated on the Nafion® 117 membrane. The novel Pd/GF anode was not bonded by hot-pressing to the membrane of the half-MEA. Furthermore, Nafion was not added to the catalyst layer and the overall MEA fabrication procedure has been simplified compared with conventional catalyst layers coated either on the membrane or onto the diffusion layer. Thus, experimental uncertainties caused by the anode catalyst layer Nafion content and hot-pressing conditions were eliminated.

The cathode diffusion-backing layer was Elat® carbon cloth (E-Tek Inc.) in all cases. In the case of the full MEA with CCM, a carbon cloth was employed as the anode backing layer whereas a backing layer was not needed in the fuel cell using the Pd/GF anode.

Both the MEA and the half-MEA were pre-conditioned before use in 0.5 M H_2SO_4 for 24 h. The estimated effective thickness of the GF anode in the fuel cell under compression was about 1.5 mm (which means about a 50% reduction of the thickness). Teflon®-coated gaskets were used at both the anode and cathode sides to assure good sealing. The DFAFC was assembled with two gold-plated end plates having serpentine flow channels.

The fuel cell tests were performed using a Fideris Inc. MTK fuel cell test station, equipped with corrosion-resistant fittings and operated using the FC Power® software. The tests were carried out at 333 K with O_2 (dry medical grade, Praxair Inc.) flow rate of 500 cm^3 min^{-1} at 2.5 bar absolute pressure on the cathode side and atmospheric pressure at the anode. The anolyte was 1 M HCOOH and 0.5 M H_2SO_4 with a flow rate of 6 cm^3 min^{-1}. The anolyte was fully recycled during the operation of the cell (i.e., multi-pass mode). The system was allowed to stabilize for 2 h and reach the operating temperature before the fuel cell polarization curve was recorded. Current was progressively drawn and the cell voltage was recorded after 10 s of operation at constant current.

For fuel cell performance comparison, full MEAs were obtained from Lynntech Inc. with 40 g m^{-2} of Pd black (anode) coated on the membrane (catalyst-coated membrane, CCM configuration) and were tested under identical conditions to the in-house prepared Pd/GF anodes.

3 Results and discussion

3.1 Pd electrodeposition on GF: the synergistic effect of Triton X-102 micellar solution and Shipley-type surface pretreatment

An electrodeposition experimental design matrix was carried out with two variables at three levels each: Triton

X-102 concentration (0, 12.5, and 25 vol%) and GF pretreatment time using the $SnCl_2$–$PdCl_2$ Shipley-type solution (0, 24, and 48 h). The composition and redox surface chemistry of the Shipley solution have been presented in Sect. 2.1. Electrodepositions were performed at 341 K, in galvanostatic mode with 20 A m^{-2} deposition superficial current density and 4.5 mM $PdCl_2$ in the plating solution.

Figure 1 summarizes the results of the experimental design matrix in terms of Pd loading and specific surface area. It is important to note without surfactant and surface pretreatment, the electrodeposited Pd flaked off easily from the GF surface during the post-deposition cleaning treatment (Sect. 2.2) and no accurate mass load or surface area measurement could be obtained. Therefore, it can be concluded that the adherence of Pd to the bare GF surface was weak.

The surface pretreatment with the Shipley method was essential for strong adherence of the electrodeposited Pd to the GF surface. The amount of Pd electrodeposited increased with pretreatment time virtually regardless of the Triton X-102 concentration (Fig. 1) as a result of the surface sensitization due to Pd(PdO) and SnO_2 formation in the Shipley-redox chemistry (Sects. 2.1 and 3.2). The addition of Triton X-102 from 0 to 12.5 vol% did not have a significant impact on the Pd mass load for the surface pretreated samples (Fig. 1), while a further increase of the surfactant content to 25 vol% actually decreased the amount of Pd deposited. The same behavior was also observed for Pt–Ru in a previous study [18].

The adsorption of surfactant aggregates block a number of possible Pd^{2+} nucleation/deposition sites thereby, improving the catalyst dispersion, while limiting the growth and stabilizing the Pd nanoparticles at diameters less than about 40 nm (Fig. 2).

The SEM images in Fig. 3 show that in the absence of Triton X-102, Pd electrodeposited as large and irregular agglomerates, coating mostly the exterior surface of the pretreated GF electrode without penetration throughout its thickness (~3 mm thick). With Triton X-102 (Fig. 4), on the other hand, the Pd particle size decreased considerably (as discussed above) forming essentially a porous Pd coating composed of particle agglomerates that was uniformly deposited in the interior of the pretreated GF electrode as well. Thus, the combination of improved surface wetting and lower electrodeposition rate induced by the Triton X-102 micelles, greatly enhanced the penetration of the Pd deposition throughout the GF electrode volume (compare Figs. 3 and 4). The highest Pd mass load (57 g m^{-2}) and specific surface area (291 m^2 m^{-2}) were obtained in the case of 12.5 vol% Triton X-102 and 48 h pretreatment time (Fig. 1).

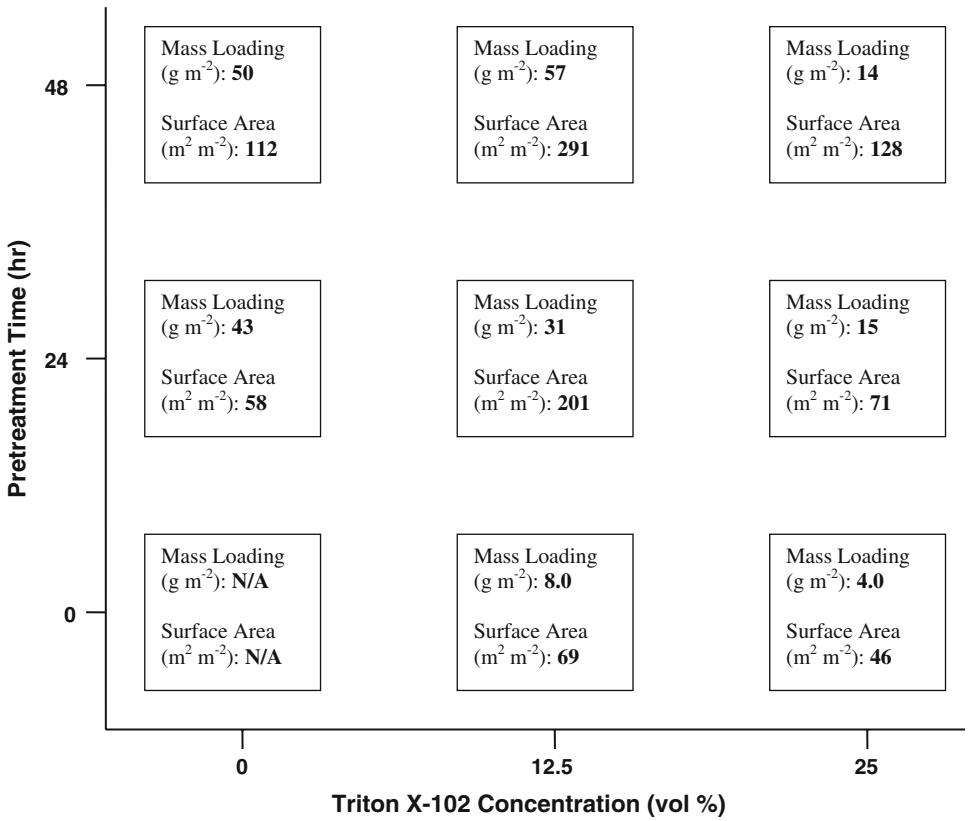

Fig. 1 Effect of Triton X-102 concentration and $SnCl_2$–$PdCl_2$ (Shipley-type solution) pretreatment time on the electrodeposited Pd mass load and Pd specific surface area. Substrate: GF. Electrodeposition conditions: temperature 341 K, $PdCl_2$ concentration 4.5 mM, deposition superficial current density 20 A m^{-2}, time 120 min

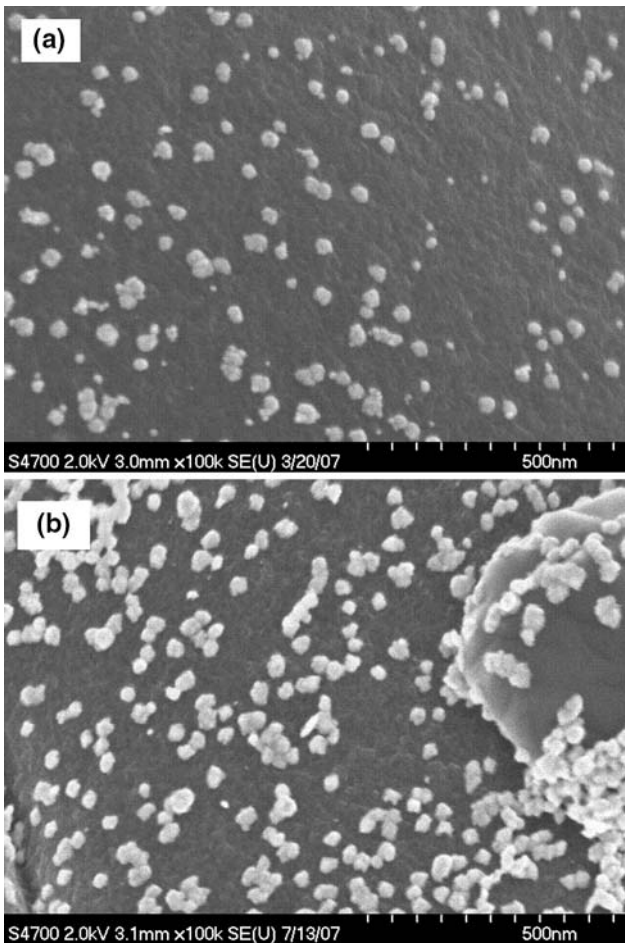

Fig. 2 SEM images of Pd electrodeposited on bare GF not pretreated by Shipley-type solution. Electrodeposition conditions: 12.5%vol Triton X-102, 341 K, 20 A m^{-2}, 120 min. **a** $PdCl_2$ concentration in the plating solution 0.75 mM. Pd mass load on GF 0.2 g m^{-2}, **b** $PdCl_2$ concentration in the plating solution 4.5 mM. Pd mass load on GF 8.0 g m^{-2}

3.2 The effect of the Shipley-type pretreatment on the graphite surface

To better understand the surface sensitization effect of the Shipley ($PdCl_2 + SnCl_2$) solution (Sect. 2.1), separate GF pretreatment experiments were performed and the GF was subjected to SEM imaging, ICP and XPS analysis to determine the Pd and Sn contents as well as the surface oxygen content.

The Pd and Sn mass load (from ICP), the Sn:Pd surface atomic ratio (from XPS) and the surface oxygen content (from XPS) are shown in Table 1 as a function of the GF pretreatment time. The deposition yield of the Shipley-type pretreatment was very low, as expected, since it is meant to act only as a surface sensitization process providing active centers for the subsequent electrodeposition. SEM imaging (Fig. 5) revealed a fairly dense surface coverage of the Pd(PdO)–SnO_2 nanoparticles ($\sim$10–30 nm diameter) acting as active centers for the subsequent Pd electrodeposition and also imparting catalyst-support interaction effects.

The Sn:Pd surface atomic ratio decreased with pretreatment time from 3.4 (after 24 h) to 2.6 (after 48 h) indicating the enhanced rate of spontaneous Pd deposition with time (Table 1). The surface oxygen content increased from 4.8 at.% without pretreatment to 26.6 at.% with 24-h pretreatment and 33.5 at.% with 48-h pretreatment (Table 1). Considering that Sn is present as SnO_2 (Eq. 3) and also some of the Pd could be oxidized to PdO, it is clear from Table 1 that the graphite surface must have oxidized as well forming various oxygenated functional groups (Sect. 2.1). This was also reflected by the change in the wetting properties of the GF. Without pretreatment the GF was hydrophobic while after pretreatment it became hydrophilic. The change in GF surface wetting properties is beneficial for both Pd electrodeposition and DFAFC anode application for enhanced liquid mass transport.

3.3 Pd electrodeposition study by voltammetry

The observations presented above with respect to the Triton X-102 and Shipley-pretreatment effects were in agreement with a voltammetry study of the Pd electrodeposition (Fig. 6). The addition of Triton X-102 suppressed significantly the rates of both H_2 evolution and Pd electrodeposition (i.e., lower deposition current density at the same potential, compare curves A and C of Fig. 6). Furthermore, in the presence of Triton X-102 a broad Pd deposition peak developed around 0.35 V (curve C, Fig. 6).

Pretreatment of the GF led also to suppression of H_2 evolution and Pd deposition rates (curve B, Fig. 6). Thus, the weak Pd attachment to graphite in case of catalyst deposited without Triton X-102 and surface pretreatment could be explained by the high rate of H_2 evolution impeding the Pd nucleation and loosening the surface adhesion of Pd. Furthermore, it is noteworthy that with Triton X-102 present, the potential domain of Pd deposition (corresponding to the broad peak in curve D, Fig. 6) was extended by about -150 mV when the surface was pretreated with the Shipley solution as compared to the unpretreated case (compare curves D and C, Fig. 6). This indicates the number of available Pd electrodeposition sites increased as a result of the surface activation by the pretreatment method.

The effect of cathode potential on the deposit morphology has been studied for various metals, such as Pt, Pd, and Zn [23, 24]. It was shown that the more negative the cathode overpotential generally the smaller the particle size. Due to the combined effect of Triton X-102 and Shipley-surface pretreatment, based on Fig. 6, the cathode

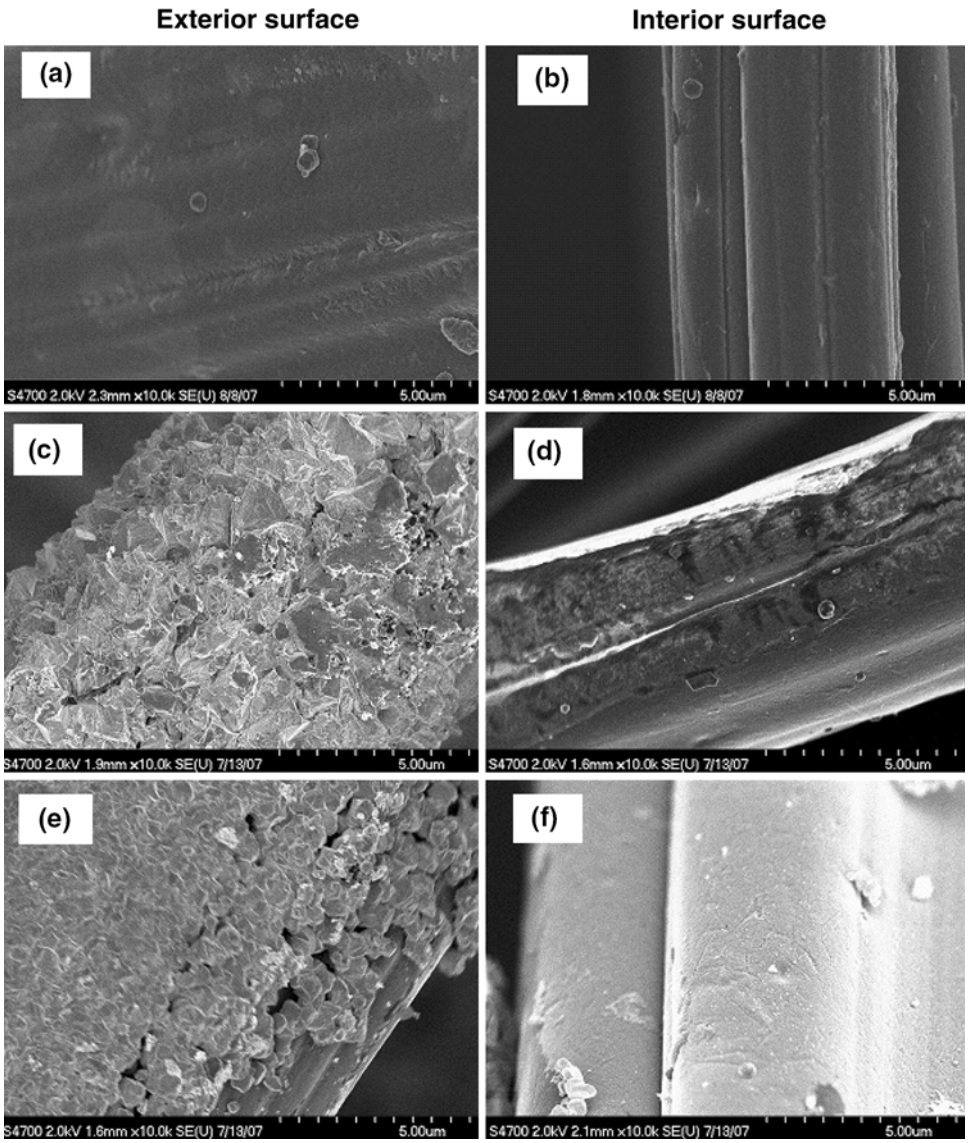

Fig. 3 SEM images of electrodeposited Pd/GF without Triton X-102. Effect of $SnCl_2$–$PdCl_2$ (Shipley-type solution) pretreatment time. Comparison of representative exterior and interior surfaces of GF. **a**, **b** no pretreatment; **c**, **d** 24 h pretreatment; **e**, **f** 48 h pretreatment

overpotentials shifted toward more negative values, i.e., −0.29, −0.33, −0.37, and −0.39 V, respectively, for cases A–D in Fig. 6, for a constant deposition current density of 20 A m^{-2} (which was used in the galvanostatic electrodeposition, Figs. 3 and 4). The equilibrium potential of Pd^{2+}/Pd at the experimental conditions was 0.88 V.

3.4 Crystallography of the electrodeposited Pd and electrochemical area estimation

Figure 7 presents the XRD spectra for the sample prepared with 48 h of pretreatment and 12.5 vol% Triton X-102. The crystallite size estimated by Scherrer's formula for Pd (1,1,1), Pd (1,0,0), Pd (1,1,0), and Pd (3,1,1), was 27.8, 19.0, 22.6, and 18.5 nm, respectively. The fractions of the different crystal planes were: 52.3% Pd (1,1,1), 21.7% Pd (1,0,0), 12.5% Pd (1,0,0), and 13.5% Pd (3,1,1).

The effective electrochemically active Pd surface area was estimated by Cu UPD (Sect. 2.3). Figure 8 shows the anodic stripping of the Cu underpotentially deposited monolayer with reference to the anodic scan of Pd/GF without Cu layer (referred to as blank). The area between the two curves was used to estimate the specific surface area of 291 m^2 m^{-2} for the electrodeposited Pd/GF when 48 h of Shipley-type surface pretreatment was employed and 12.5 vol% Triton X-102 was present in the plating solution.

3.5 Intrinsic catalytic activity of electrodeposited Pd/GF toward formic acid oxidation

The cyclic voltammogram in Fig. 9 shows the Pd/GF prepared without Triton X-102 had a very high formic acid oxidation onset potential (0.6 V) in contrast to the sample

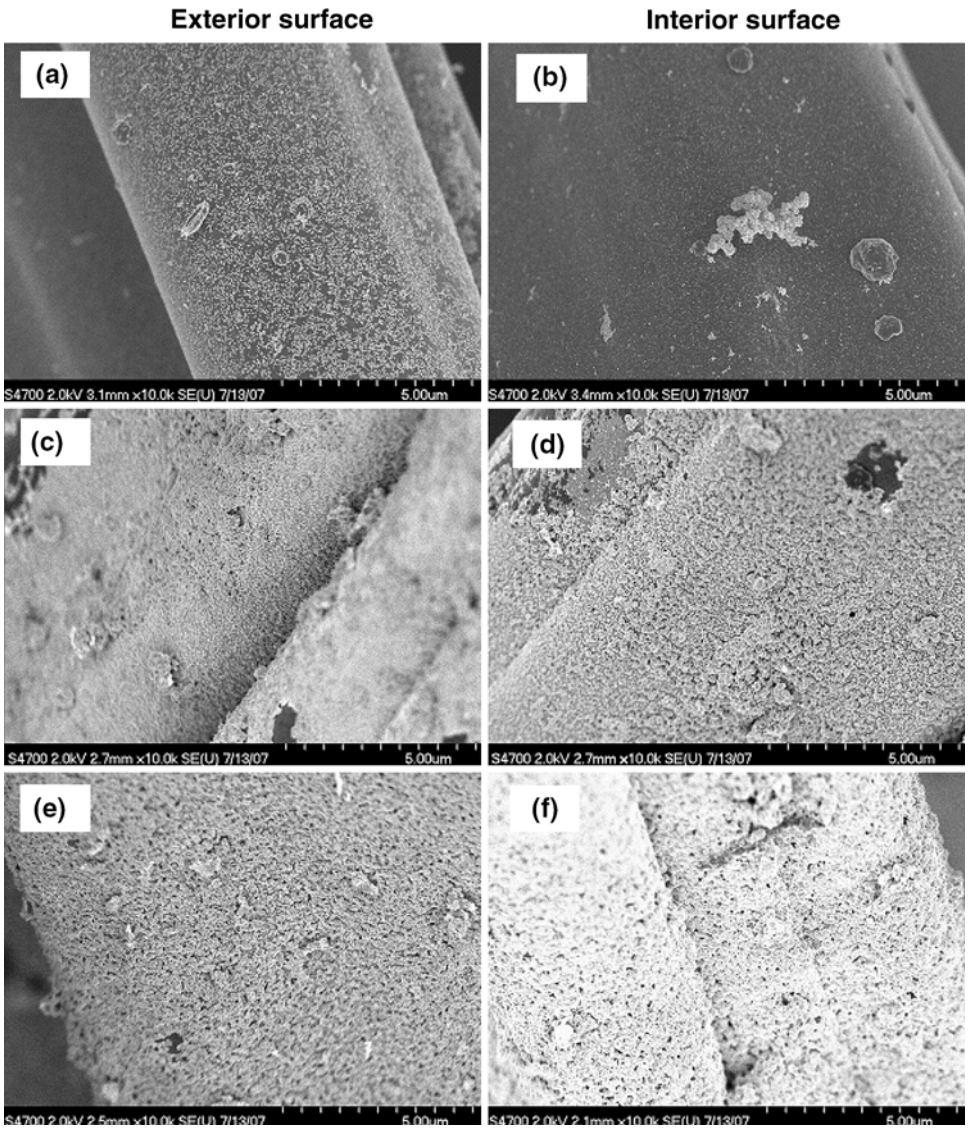

Fig. 4 SEM images of electrodeposited Pd/GF with 12.5 vol% Triton X-102. Effect of $SnCl_2$-$PdCl_2$ (Shipley-type solution) pretreatment time. Comparison of representative exterior and interior surfaces of GF **a**, **b** no pretreatment; **c**, **d** 24 h pretreatment; **e**, **f** 48 h pretreatment

prepared with Triton X-102. The difference can be explained by the particle size and roughness of the electrodeposited Pd. As revealed by the SEM images, the Pd/GF prepared in the absence of Triton X-102 was made up of large and relatively smooth agglomerates ($\sim$1,000 nm, Fig. 3c) whereas the sample prepared with 25 vol% Triton X-102 was composed of nanoparticles (diameter <40 nm) (Fig. 4a).

In the case of large and smooth Pd agglomerates produced without surfactant, the formic acid cyclic voltammetry characteristics (onset potential at $\sim$0.6 V and a pronounced hysteresis loop on the reverse scan with much higher oxidation current, Fig. 9 curve A) were essentially the same as that of formic acid oxidation on Pt published by Liu et al. [25]. Thus, the large and smooth Pd surface exhibited a Pt-like behavior with respect to formic acid oxidation. Conversely, the Pd nanoparticles with rough surface deposited with Triton X-102, were much more active, with an oxidation onset potential around 0.1 V. Moreover, the current density on the reverse scan was virtually identical with the forward scan at potentials below 0.6 V (i.e., no hysteresis loop) suggesting the removal of CO_{ad} at high potentials was not an issue.

These results indicate that differences in catalyst morphology caused the formic acid oxidation reaction to follow different reaction pathways: smooth and large Pd particles behaving like Pt and the oxidation proceeding via the CO_{ad} pathway in contrast to the non-CO_{ad} pathway for nano-sized Pd with rough surface.

Interestingly, Pd/GF prepared with surfactant and Shipley-type surface pretreatment, exhibited current-oscillation behavior at high potentials (>1.0 V) (Fig. 10) in contrast to the catalyst synthesized without either surfactant or pretreatment (Fig. 9). Possible electronic

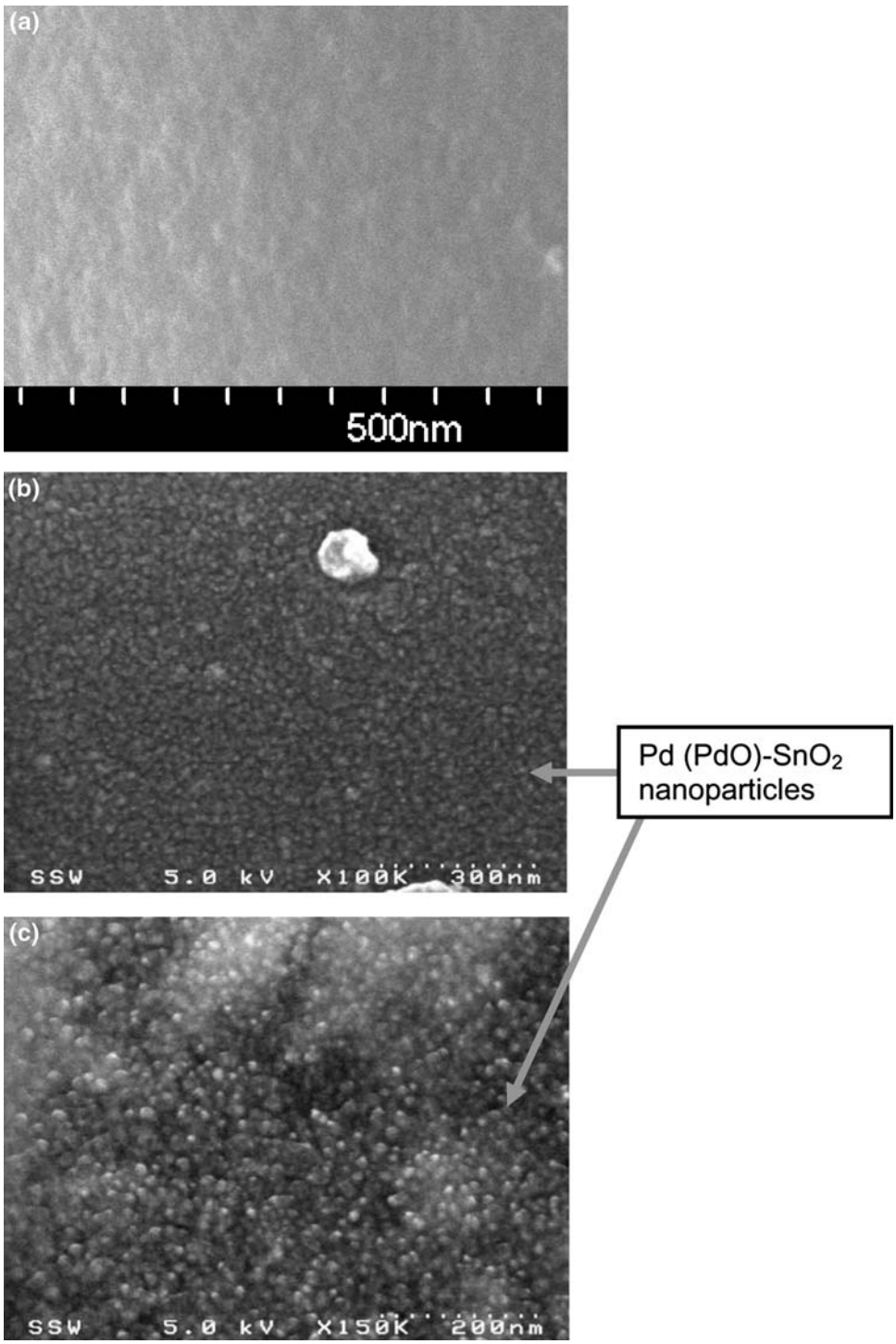

Fig. 5 The effect of Shipley-type solution pretreatment on a representative interior surface of GF. **a** no pretreatment, **b** 24 h pretreatment and **c** 48 h pretreatment

interactions between the electrodeposited Pd nanoparticles and the Pd(PdO)–SnO_2 support (generated by Shipley treatment) could play a role in the apparition of the oscillatory behavior at E >1.0 V. Current oscillations during formic acid oxidation have been observed and studied by various researchers [26–29]. The phenomenon has been explained by the periodic adsorption and removal of various proposed surface poisons. Arenz et al. [10, 30] invoked OH_{ad} as the predominant surface poison at high potentials where the dehydrogenation pathway is prevalent.

Figure 11 summarizes the intrinsic catalytic activity (expressed as current per electrochemically active area) at 0.3 V for the Pd/GF samples prepared with different concentrations of Triton X-102 and Shipley solution pretreatment time. The intrinsic catalytic activity toward formic acid oxidation increased with the presence of Triton X-102,

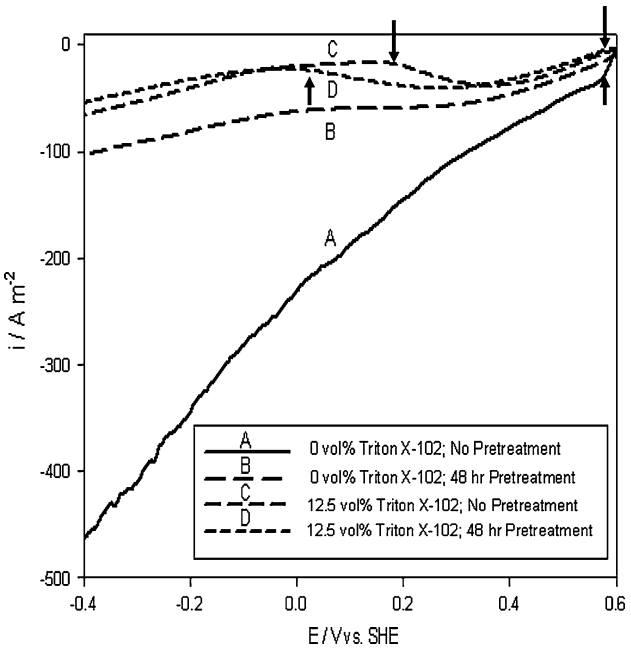

Fig. 6 Voltammograms of Pd electrodeposition on GF. Effect of Triton X-102 content and Shipley-type surface pretreatment. $PdCl_2$ concentration: 4.5 mM. Temperature: 341 K. Scan rate: 5 mV s^{-1}

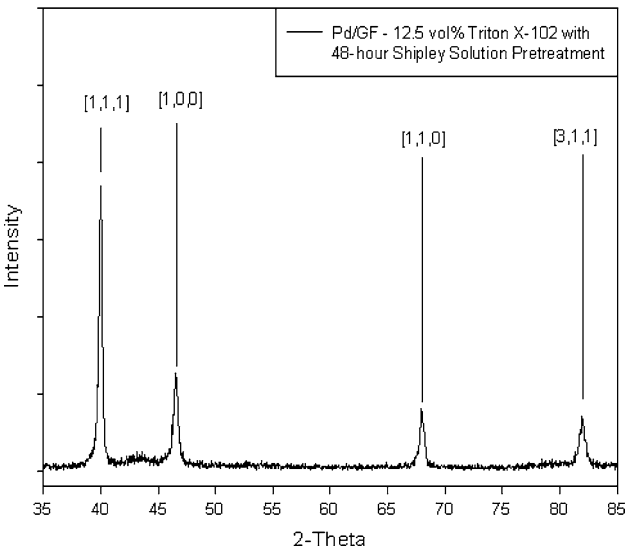

Fig. 7 XRD spectra of electrodeposited Pd/GF after 48 h of Shipley-type solution pretreatment. Electrodeposition conditions: 12.5 vol% Triton X-102; 20 A m^{-2}; 341 K

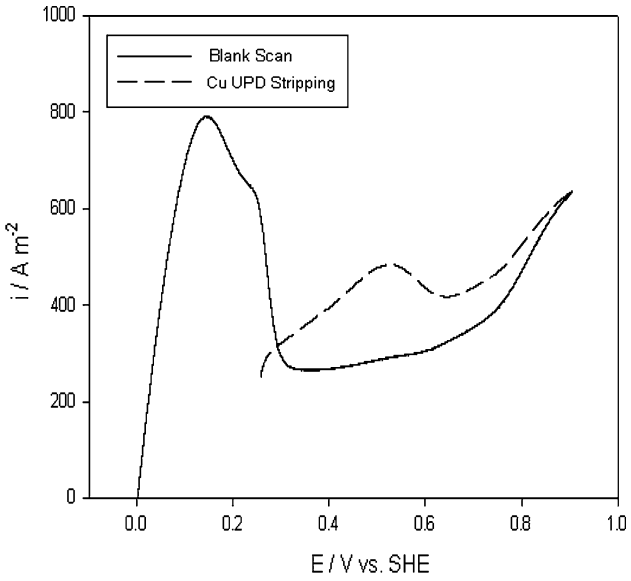

Fig. 8 Voltammetric anodic scans of Pd/GF and Cu underpotential deposited/Pd/GF. Pd/GF was electrodeposited in the presence of 12.5 vol% Triton X-102 after 48 h of Shipley solution pretreatment. Test solution: 0.5 M H_2SO_4 (*blank*); 0.5 M H_2SO_4 + 0.002 M $CuSO_4$ (*Cu UPD*) Temperature: 298 K; Scan rate: 50 mV s^{-1}

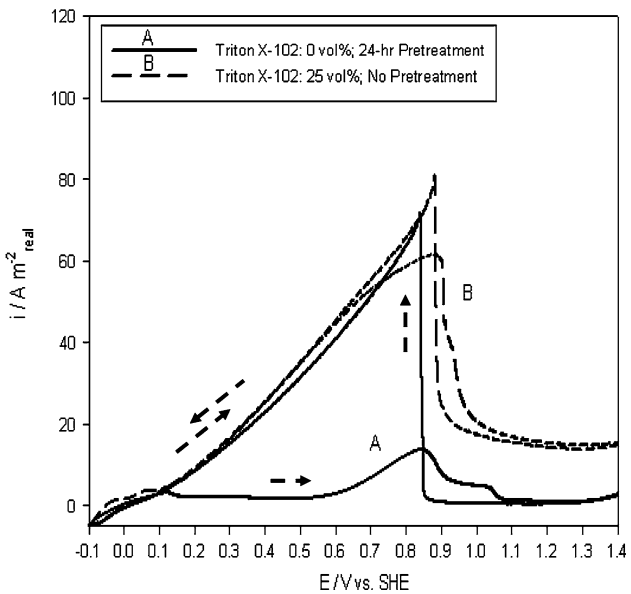

Fig. 9 Cyclic voltammograms of formic acid electro-oxidation using Pd electrodeposited on GF. **a** no Triton X-102 and 24-h pretreatment; **b** 25 vol% Triton X-102 and no pretreatment. Electrolyte: 1 M HCOOH and 0.5 M H_2SO_4. Temperature: 298 K. Scan rate: 5 mV s^{-1}

which was also shown for Pt–Ru/GF [18]. It is interesting to note the effect of Shipley solution pretreatment. In the cases without surfactant, treating the GF surface with Shipley solution for 48 h as opposed to 24 h improved the catalytic activity (Fig. 11) due to somewhat smaller and more uniform Pd deposit formation (Fig. 3c and e). However, in the cases with Shipley pretreatment as well as the presence of Triton X-102 during electrodeposition, it is evident from Fig. 11 that the oxidation current per real electrochemically active area decreased with Shipley solution pretreatment time. In this case the beneficial Pd morphology is offset by potential support-catalyst

electronic interaction effects induced by the presence of SnO_2 decreasing the intrinsic kinetic activity of Pd. Hence, the Shipley pretreated surface can be regarded as a special support and the catalyst system in this case is Pd/SnO_2–Pd(PdO)/GF (with partial oxidation).

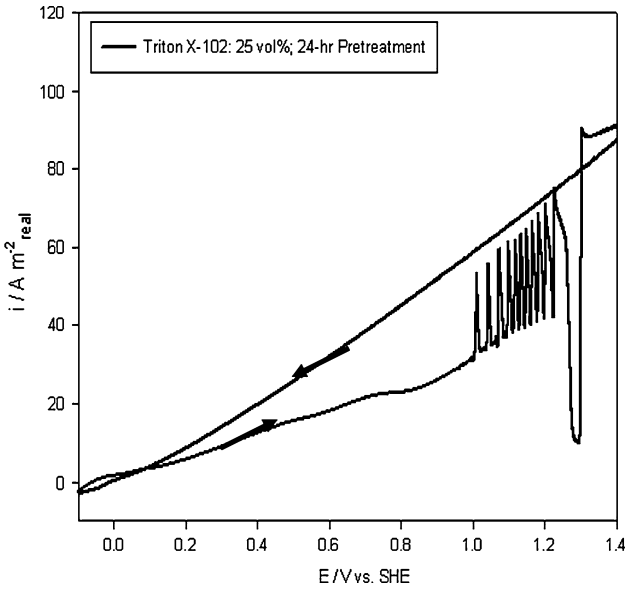

Fig. 10 Oscillatory phenomena during formic acid electro-oxidation using Pd electrodeposited on GF prepared with 25 vol% Triton X-102 with 24-h Shipley pretreatment. Electrolyte: 1 M HCOOH and 0.5 M H_2SO_4. Temperature: 298 K. Scan rate: 5 mV s^{-1}

3.6 Catalytic activity and long-term stability of Pd/GF: comparison with Pt–Ru

On geometric electrode area basis, the highest oxidation current density (referred to also as superficial current density) was obtained for the Pd/GF prepared with 12.5 vol% Triton X-102 after 48 h of pretreatment (Fig. 12). This is due to the high specific surface area and excellent penetration throughout the GF electrode (Fig. 4c and d), offsetting the lower intrinsic kinetic activity, as discussed in Sect. 3.5, of the Shipley pretreated surface. Therefore, the Pd/GF catalyst electrodeposited with 12.5 vol% Triton X-102 after 48 h of pretreatment (in effect Pd/SnO_2–Pd(PdO)/GF(with partial oxidation)) was retained for further investigations since one of the objectives was to increase the formic acid fuel cell power density.

In order to evaluate the applicability of Pd/GF as DFAFC anode, the catalytic activity and long-term stability toward formic acid electro-oxidation were first studied by chronoamperometry and compared to Pt–Ru/GF prepared using the same micellar electrodeposition media [18]. The higher initial catalytic activity of Pd was not sustained over more than approximately 1 h of continuous operation at 0.65 V_{SHE} (Fig. 13). The catalytic activity of Pd/GF declined steadily resulting in a total drop in current density of 79% in 3 h. On the other hand, Pt–Ru/GF retained

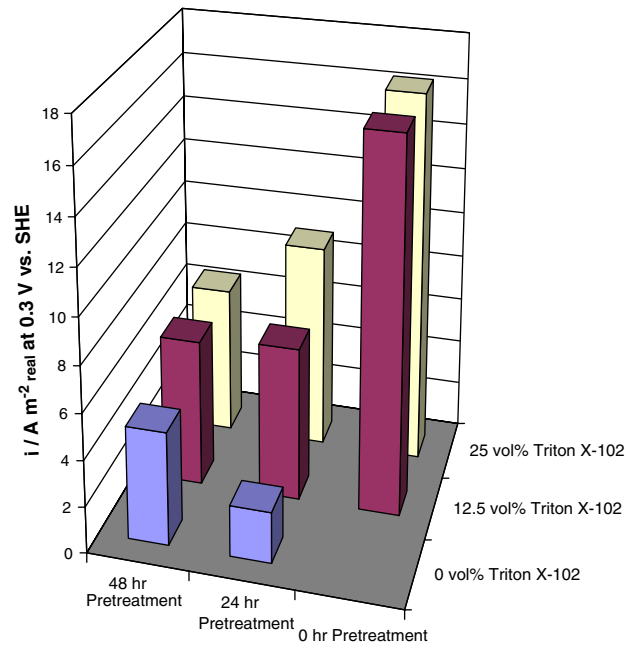

Fig. 11 Formic acid oxidation current density on Pd/GF expressed per real electrochemically active area (intrinsic catalytic activity). Electrolyte: 1 M HCOOH and 0.5 M H_2SO_4. Temperature: 298 K

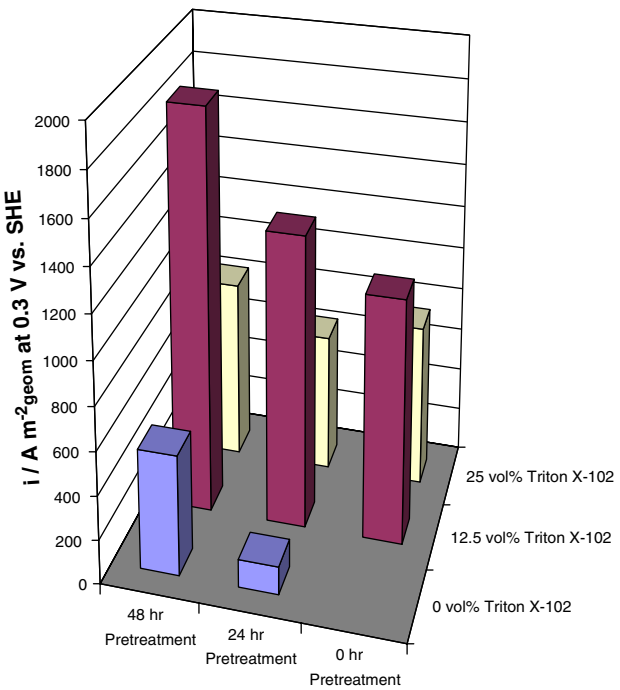

Fig. 12 Superficial (i.e., per geometric area) formic acid oxidation current density on Pd/GF. Electrolyte: 1 M HCOOH and 0.5 M H_2SO_4. Temperature: 298 K

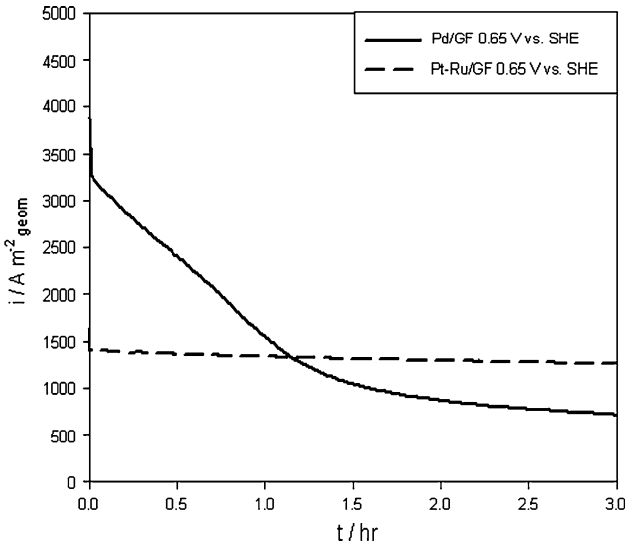

Fig. 13 Chronoamperometry of formic acid electro-oxidation using Pt–Ru and Pd electrodeposited on GF. Electrolyte: 3 M HCOOH and 0.5 M H_2SO_4. Temperature: 298 K. Potential: 0.65 V versus SHE

approximately 86% of its initial current density even after 3 h.

The rate of Pd deactivation shown by Fig. 13 is in agreement with literature publications by various researchers. Li and Hsing [2] prepared Pd supported on Vulcan XC-72R by a surfactant-stabilized method. The Pd/C lost 90% of its initial oxidation current density in 20 min. Similarly, Larsen et al. [9] reported data for an Alfa Aesar commercial Pd black catalyst at 0.3 V showing that the current density decreased by 80% after 1 h and 95% after 3 h of operation. The deactivation was proposed to be the result of reaction intermediate adsorption. Clearly more studies are required to gain a better understanding of the Pd deactivation mechanism as a function of crystallographic features, particle size and surface roughness.

3.7 DFAFC performance

Figures 14 and 15 show comparative DFAFC polarization and power density curves at 333 K. The following four anodes are compared: Pd/GF (prepared by electrodeposition with 12.5 vol.% Triton X-102 and 48 h of Shipley-type surface pretreatment), Pt–Ru/GF (prepared by electrodeposition with 12.5 vol.% Triton X-102) [18], commercial Pd CCM, and commercial Pt–Ru CCM [18]. For the GF anode structures, (effective thickness in fuel cell under compression of $\sim$1.5 mm) 0.5 M H_2SO_4 was used as supporting electrolyte to reduce the ohmic voltage loss.

The steady-state open circuit voltage (OCV) of commercial Pd CCM and Pd/GF were similar, about 0.84 V. The corresponding OCV of Pt–Ru catalyst (either CCM or supported on GF) was only 0.64 V. Thus, regardless of

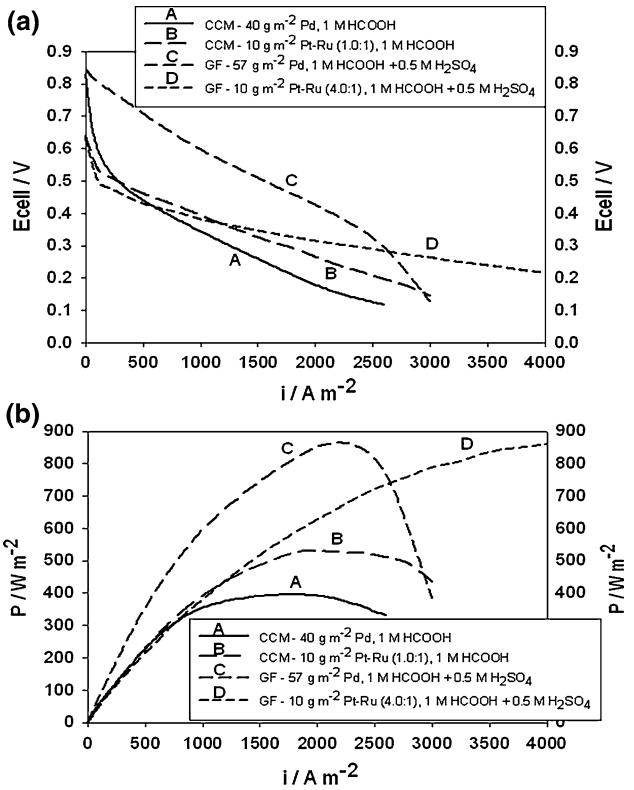

Fig. 14 DFAFC performance. Anolyte: 1 M HCOOH and 0.5 M H_2SO_4, atmospheric pressure. Flow rate 6 cm^3 min^{-1}. Cathode: 40 g Pt m^{-2}, dry O_2 fed at 2.5 bar and 500 cm^3 min^{-1}. Temperature: 333 K. **a** Polarization curve; **b** Power density. *Note*: Pd/GF was prepared by electrodeposition with 12.5 vol% Triton X-102 and 48 h of Shipley-type surface pretreatment

electrode design, the OCV of Pd was significantly higher than Pt–Ru, which is in agreement with the more negative onset potential for formic acid oxidation on Pd. For the CCM anodes Pd gave higher cell voltages than Pt–Ru in the low current density region (up to 300 A m^{-2}, curves A and B Fig. 14) due to better kinetics and hence lower activation overpotential for formic acid oxidation on Pd than on Pt–Ru. For current densities greater than 300 A m^{-2}, interestingly Pt–Ru CCM with four times lower catalyst load performed better than Pd CCM (curves A and B Fig. 14). This could indicate Pd deactivation at high current densities increasing the anode overpotential. The results agreed well with those presented by Rice et al. [31] for Pt–Ru.

Comparing the fuel cell polarization curves for Pd/GF and Pd CCM (curves C and A, Fig. 14), the novel extended reaction zone electrode provided significantly better performance over the entire polarization curve. Further research is required to elucidate the differences in intrinsic electrode kinetic behavior between Pd nanoparticles in the CCM configuration produced by a thermochemical method and the Pd nanostructures generated by the novel

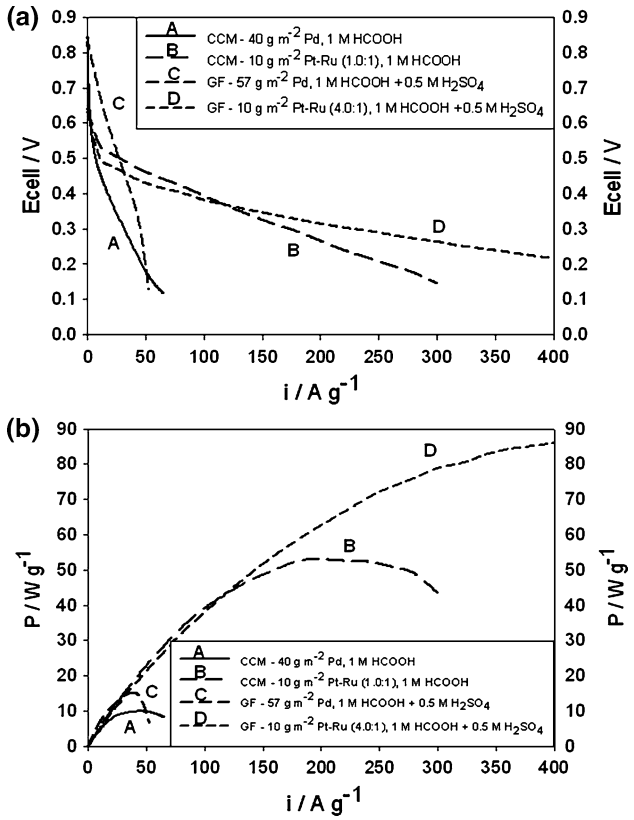

Fig. 15 DFAFC performance in terms of anode catalyst mass-specific activity. Conditions *idem* Fig. 14

electrodeposition method and supported on GF. It is possible that catalyst-support electronic interactions, particle size effects, surface roughness, and other catalyst morphology aspects, as discussed in Sect. 3.5, might play an important role.

The mass transfer limiting current density for Pd/GF was high, 2,500 A m^{-2} (Fig. 14) showing clearly the advantageous mass transfer in a two-phase flow situation. The peak power density based on geometric electrode area was 852 W m^{-2} for Pd/GF versus 392 W m^{-2} for Pd CCM (Fig. 14) or alternatively on Pd mass-specific basis 15 W g^{-1} Pd/GF versus 9.8 W g^{-1} Pd CCM (Fig. 15). These results are clearly demonstrating the effectiveness of the novel anode structure in case of the Pd catalyst as well in addition to Pt–Ru [18]. However, as shown by Fig. 15 it is important to note that the anode catalyst mass-specific peak power of Pt–Ru was superior compared to Pd for both GF and CCM (compare curves C and D or A and B in Fig. 15).

Concurring with the half-cell electrochemical study, deactivation of Pd was evident in fuel cell experiments as well. While the performance of the Pt–Ru catalysts was essentially steady during the experiment, the cell voltage of the Pd-based DFAFC decreased on average at a rate of approximately 1 mV s^{-1} at current densities higher than 200 A m^{-2}. Preliminary results showed that Pd/GF had somewhat better stability than Pd CCM. Again, more studies are required to understand the relationship between catalyst morphology and preparation method with respect to long-term stability.

4 Conclusion

The galvanostatic electrodeposition of Pd on GF (thickness ~3 mm in uncompressed state) was investigated using a Triton X-102 micellar solution. Pretreatment of the GF with a Shipley-type solution ($PdCl_2$+$SnCl_2$) in conjunction with the use of Triton X-102 micellar media was essential to obtain uniformly dispersed Pd nanoparticles (diameter <40 nm) throughout the thickness of the GF. The pretreatment method induced the formation of Pd(PdO)–SnO_2 on the graphite surface acting as centers for Pd electrodeposition and creating a different catalyst-support interaction effect. It was found that the Pd catalyst morphology (i.e., large ~1,000 nm particles with smooth surface versus nanoparticles (diameter <40 nm) with rough surface) had a pronounced effect on the formic acid oxidation pathway.

In DFAFC experiments, the advantage of the novel GF (extended reaction zone) anode was clearly demonstrated. With Pd/GF (57 g m^{-2}) prepared in the presence of 12.5 vol% Triton X-102 and 48 h of Shipley-type pretreatment, a maximum power output on a geometric area basis of 852 W m^{-2} was obtained at 333 K compared to 392 W m^{-2} obtained with a commercial CCM loaded with 40 g m^{-2} Pd. However, from both half-cell electrochemical and fuel cell experiments, it was evident that Pt–Ru/GF is a more promising catalyst compared to Pd due to its superior long-term stability.

Acknowledgments The authors thank Dr. Elaine Humphrey of UBC BioImaging facility for the use of the SEM equipment, Dr. Anna Ignaszak of UBC for XRD, and Dr. Anna Becalska of CanTest for ICP-AES. The financial support by the Natural Sciences and Engineering Research Council of Canada is also gratefully appreciated.

References

1. Zhang LJ, Wang ZY, Xia DG (2006) J Alloys Compd 426:268
2. Li X, Hsing IM (2006) Electrochim Acta 51:3477
3. Choi JH, Jeong KJ, Dong Y, Han J, Lim TH, Lee JS, Sung YE (2006) J Power Sources 163:71
4. Capon, Parsons R (1973) J Electroanal Chem 45:205
5. Chen YX, Heinen M, Jusys Z, Behm RJ (2006) Angew Chem Int Ed 45:981
6. Markovic NM, Gasteiger HA, Ross PN, Jiang X, Villegas I, Weaver MJ (1995) Electrochim Acta 40:91

7. Weber M, Wang JT, Wasmus S, Savinell RF (1996) J Electrochem Soc 143:L158
8. Capon D, Parsons R (1973) Electroanal Chem Interfacial Electrochem 44:239
9. Larsen R, Ha S, Zakzeski J, Masel RI (2006) J Power Sources 157:78
10. Arenz M, Stamenkovic V, Schmidt TJ, Wandelt K, Ross PN, Markovic NM (2003) Phys Chem Chem Phys 5:4242
11. Blair S, Lycke D, Iordache C (2006) Electrochem Soc Trans 3:1325
12. Zhu Y, Khan Z, Masel RI (2005) J Power Sources 139:15
13. Wilkinson DP, Johnson MC, Colbow KM and Campbell SA (1999) US Patent 5,874,182, 13 Feb 1999
14. Bauer EL, Gyenge, Oloman CW (2006) Electrochim Acta 5:5356
15. Bauer EL, Gyenge, Oloman CW (2007) J Power Sources 16:281
16. Cheng TT, Gyenge EL (2006) Electrochim Acta 51:3904
17. Cheng TT, Gyenge EL (2008) J Appl Electrochem 38:51
18. Cheng TT, Gyenge EL (2008) J Electrochem Soc 155:B819
19. Chetty R, Scott K (2007) J New Mater Electrochem Syst 10:135
20. Tran TD, Langer SH (1993) Electrochim Acta 38:1551
21. Egan RW, Jones MA, Lehninger AL (1976) J Biol Chem 251:4442
22. Rusanova MY, Tsirlina GA, Petrii OA, Safonova TY, Vasil'ev SY (2000) Russ J Electrochem 36:457
23. Chetty R, Scott K (2007) J New Mater Electrochem Syst 10:135
24. Jayashree RS, Spendelow JS, Yeom J, Rastogi C, Shannon MA, Kenis PJA (2005) Electrochim Acta 50:4674
25. Liu Z, Hong L, Tham MP, Lim TH, Jiang H (2006) J Power Sources 161:831
26. Samjeske G, Osawa M (2005) Angew Chem Int Ed 44:5694
27. Samjeske G, Miki A, Ye S, Yamakata A, Mukouyama Y, Okamoto H, Osawa M (2005) J Phys Chem B 109:23509
28. Samjeske G, Miki A, Ye S, Osawa M (2006) J Phys Chem B 110:16559
29. Lang GG, Seo M, Heusler KE (2005) J Solid State Electrochem 9:347
30. Arenz M, Stamenkovic V, Ross PN, Markovic NM (2004) Surf Sci 573:57
31. Rice S, Ha RI, Masel A, Wieckowski (2003) J Power Sources 115:229